








RESEARCH ARTICLE | JUNE 14 2024

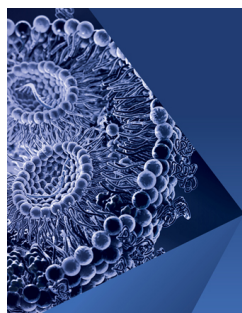
Impact of reduced gravity on food mixing and emptying in human stomach: A numerical simulation study

Changyong Li (李昌勇)  ; Xiao Dong Chen (陈晓东) ; Jie Xiao (肖杰) ; Renpan Deng (邓人攀) ; Yan Jin (金琰)  



Physics of Fluids 36, 061908 (2024)

<https://doi.org/10.1063/5.0208898>



Physics of Fluids

Special Topic:

Flow and Lipid Nanoparticles

Guest Editors: Richard Braatz and Mona Kanso

Submit Today!

Impact of reduced gravity on food mixing and emptying in human stomach: A numerical simulation study

Cite as: Phys. Fluids **36**, 061908 (2024); doi: [10.1063/5.0208898](https://doi.org/10.1063/5.0208898)

Submitted: 18 March 2024 · Accepted: 30 May 2024 ·

Published Online: 14 June 2024



View Online



Export Citation



CrossMark

Changyong Li (李昌勇),^{1,2,a)} Xiao Dong Chen (陈晓东),³ Jie Xiao (肖杰),³ Renpan Deng (邓人攀),⁴ and Yan Jin (金琰)^{5,a)}

AFFILIATIONS

¹Fujian Provincial Key Laboratory of Biochemical Technology & Institute of Biomaterials and Tissue Engineering, College of Chemical Engineering, Huaqiao University, Xiamen 361021, China

²Center of Applied Space Technology and Microgravity (ZARM), University of Bremen, Am Fallturm 2, Bremen 28359, Germany

³Life Quality Engineering Interest Group, School of Chemical and Environmental Engineering, College of Chemistry, Chemical Engineering and Materials Science, Soochow University, Suzhou 215123, China

⁴School of Chemistry and Chemical Engineering/Key Laboratory for Green Processing of Chemical Engineering of Xinjiang Bingtuan, Shihezi University, Shihezi 832003, China

⁵Institute of Multiphase Flows, Hamburg University of Technology, Hamburg 21073, Germany

^{a)}Authors to whom correspondence should be addressed: changyong.li@hqu.edu.cn and yan.jin@tuhh.de

ABSTRACT

Gravitational conditions in space diverge significantly from those experienced on Earth, and these alterations may have significant effects on gastric digestion, ultimately affecting the health of astronauts. To understand these effects, the behavior of mixing and emptying in the human stomach under both reduced and normal gravity is investigated numerically. The solver utilized in this study is developed based on the open-source toolbox OpenFOAM. The gastric contents consist of water and a soluble food bolus characterized by a density of 1100 kg m^{-3} , viscosity of $10^{-5} \text{ m}^2 \text{ s}^{-1}$, and diffusivity of $3.09 \times 10^{-9} \text{ m}^2 \text{ s}^{-1}$. The effects of gravity magnitude, initial food bolus location, and terminal antral contractions (TACs) are studied. The numerical results demonstrate that the food retention rate can be increased by up to $\sim 20\%$ in the initial 6 min as normal gravity is reduced to zero gravity. The numerical results support that gravity favors the emptying of the food through the pylorus. The distributions of food concentrations and pH are also significantly influenced by the gravity condition. Under zero gravity conditions, food in the distal stomach is quickly emptied due to the strong flow dynamics in the antrum. A delay of approximately 6 min is observed when the food bolus is initially located in the proximal stomach. TACs efficiently enhance the emptying and mixing of the food in the distal stomach, while their effects on the proximal stomach are marginal.

Published under an exclusive license by AIP Publishing. <https://doi.org/10.1063/5.0208898>

I. INTRODUCTION

Humans have long dreamed of traveling to and inhabiting outer space or other planetary bodies. Astronauts or tourists do not experience gravity while orbiting in space. Even after landing on the Moon or Mars, humans will live under much lower gravity than that of the Earth. Prolonged habitation under reduced gravity has deleterious effects on human health.¹ An important problem encountered is space adaptation syndrome (SAS).² Symptoms of SAS include nausea, vomiting, vertigo, headaches, lethargy, and overall malaise.³ SAS poses a particularly serious problem during the initial hours of weightlessness.⁴

Although weightlessness can have a significant impact on human health by affecting the digestion system, the influence of reduced gravity on gastric digestion remains unclear. As a major step of digestion in human body, gastric digestion plays a crucial role. Extensive studies are demanded to gain a clear understanding of gastric digestion in humans under reduced gravity.

The human stomach can be roughly divided into two parts: the proximal part, which mainly functions as a reservoir for undigested materials,⁵ and the distal part, which acts primarily as a grinder, mixer, and sieve for solid particles.⁶ The disintegration of ingested food is

facilitated by a series of periodically occurring antral contractions, consisting of antral contraction waves (ACWs) and terminal antral contractions (TACs). Research with respect to gastric digestion can be traced back 300 years.⁷ However, it is only in recent years that detailed investigations of the gastric digestion process have become possible due to the emergence of new experimental and numerical techniques. One emerging experimental technique involves developing realistic *in vitro* gastric models, which have been well reviewed in the literature.^{8,9} To date, there are still no experimental studies on gastric digestion under reduced gravity, mainly because experiments under reduced gravity are extremely difficult and expensive. Even with a drop tower or reduced-gravity aircraft, weightless conditions can only be achieved for a few seconds, which is far from the timescale required for real digestion.

The computational fluid dynamics (CFD) method is another important tool for investigating gastric flows in detail. Simplified yet insightful CFD models of gastric biomechanics and digestion have been developed. For instance, Pal *et al.*¹⁰ constructed a simplified two-dimensional (2D) model of the human stomach geometry and motility. They investigated the flow behavior of a Newtonian fluid with viscosity of 1.0 Pa s and observed retrograde “jets” through ACWs and circulatory flow between ACWs. Dufour *et al.*¹¹ explored how stomach contractions impact the breakup of liquid drops using models and simulations, finding that viscosity affects drop breakup and identifying specific breakup conditions. Feigl and Tanner¹² conducted a parametric study to assess the impact of interfacial tension, viscosity ratio, relative occlusion, and initial drop position on the behavior and breakup characteristics of the drop. Ferrua and Singh¹³ developed a three-dimensional (3D) model and used it to analyze the dynamics of two Newtonian fluids, which have the viscosities 1.0×10^{-3} and 1.0 Pa s. Trusov *et al.*¹⁴ studied a multiphase flow that incorporated functions of secretory, motor, and absorption in the antroduodenal portion of the gastrointestinal tract. Each phase was represented by a Newtonian fluid with varying viscosities. Harrison *et al.*¹⁵ investigated the mixing and emptying behavior of three aqueous liquid contents within the initial few minutes using a coupled biomechanical-smoothed particle hydrodynamics (B-SPH) model. The liquid contents were seen as Newtonian fluids with viscosities of 1.0×10^{-2} , 1.0×10^{-1} , and 1.0 Pa s, respectively. Ishida *et al.*¹⁶ examined the effects of impaired coordination between antral contraction and pyloric closure, considering gastric contents as Newtonian liquids with viscosity values ranging from 4.2×10^{-3} to 4.2 Pa s. The Mittal group simulated the drug dissolution in water^{17,18} and studied the impact of gastric motility on food digestion and stomach emptying¹⁹ using the immersed boundary method.

In our recent studies, we have investigated the hydrodynamics of liquid contents,²⁰ species transport, and the “Magenstrasse” for gastric mixing and emptying,²¹ as well as the digestion of meat proteins.²² The numerical study confirms that heavy food particles drop to the distal stomach shortly after ingestion. However, food particles are no longer heavier than the gastric fluid under zero gravity. There is still limited knowledge regarding how gravity affects the digestion, e.g., how food particles with different properties behave and how the pH of gastric contents distributes under reduced gravity.

The study aims to enhance our understanding of the gastric mixing and emptying mechanisms under reduced gravity. It will be carried out using a CFD method, which will be introduced in Sec. II. The detailed description of the test cases utilized in this study is described

in Sec. III. The effects of reduced gravity on gastric mixing and emptying, as revealed by the numerical results, are discussed in Sec. IV. Finally, Sec. V presents the conclusions drawn from the study.

II. COMPUTATIONAL MODEL

The digestion in human stomach is an extremely complicated process. To simulate this process, certain reasonable hypotheses and simplifications need to be made. The key ones are summarized as follows:

- The actual contraction rate of the pylorus can reach up to 90%, it might induce extremely complex flows.²³ However, in this study, the pylorus is assumed to be open and its contraction is not considered. This assumption is reasonable when water-like gastric contents are emptied.²⁴ In addition, the present study neglects tonic contractions, which refer to weak continuous contractions of the stomach wall. This simplification was primarily due to our study's focus on the lower stomach regions and their roles in gastric emptying under different gravitational conditions. Additionally, the volume of the stomach fundus does not change significantly during the initial period of digestion.
- Real food boluses are commonly cohesive, exhibiting properties that resemble those of soft solids.^{25,26} Here, the food boluses are treated as unlinked small particles, modeled as soluble species.²⁷
- Real gastric juice comprises various complex components, e.g., water, hydrochloric acid, electrolytes, mucus, and enzymes. Here, the gastric juice is simplified to contain only water and hydrogen ions (H^+ , the active component responsible for activating digestive enzymes). These are the most important aspects for the functionality of the gastric juice, while the other components are neglected.

The assumptions described earlier simplify and accelerate the simulation considerably, while the main characteristics of the stomach digestion process still can be captured.

A. Geometry and motilities of the human stomach model

The size and shape of human stomach do not have a unique description and vary individually.²⁸ A simplified 3D model that represents the postprandial state of a human stomach is shown in Fig. 1(a). It has a volume of 1.17 L, which falls within the normal capacity range of stomach, i.e., 0.25 to 1.7 L.²⁹ The diameter of the pylorus is 20.4 mm, which falls within the range observed in previous studies.²⁰ Details regarding the geometry construction can be found in Appendix A.

ACWs and TACs are schematically illustrated in Fig. 1(b) (Multimedia view). Each ACW is modeled as a series of rings with different diameters, which press against the stomach surface and move toward the terminal antrum at the speed of u_{ACW} . The imaginary centerline is indicated by the white dashed line. Points S and E indicate the center where ACWs start and end, respectively. P represents the center of the pylorus (outlet). TACs are segmental contractions of the terminal antrum, which occur when ACWs reach the terminal antrum.²⁸ Since TACs have shorter period of contractions and relaxations than ACWs and are more occluded,¹⁶ they are modeled as additional contractions and relaxations in the last 4 s of every ACW. Previous studies have shown that TACs are crucial for generating

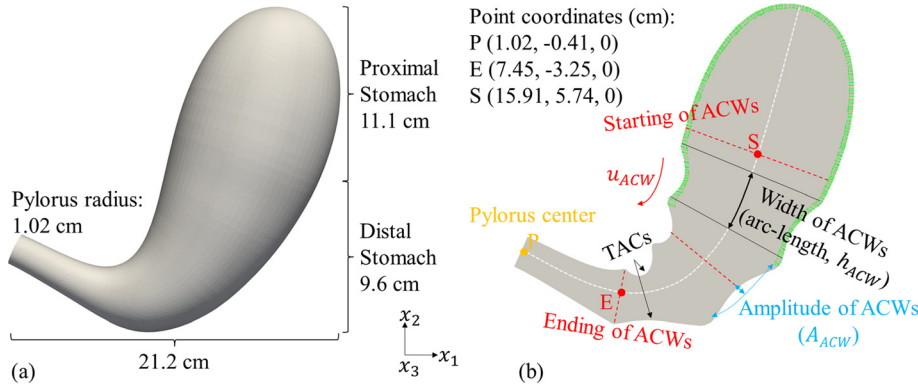


FIG. 1. (a) 3D geometry of the human stomach model, (b) schematic description of the dynamics of the contraction waves, including ACWs and TACs, the green region represents the area of the gastric juice secretion. More details on the geometrical construction and mathematical description of gastric motilities can be found in [Appendix A](#). Multimedia available online.

high-velocity retropulsive flows,^{22,30} which are beneficial for mixing and breaking down large food particles. The deformation of the computational domain due to ACWs and TACs is modeled using dynamic mesh techniques. The detailed equations describing stomach motility can be found in [Appendix A](#).

B. Governing equations

The governing equations that describe the conservation of mass, momentum, food bolus, and H^+ are given by the following equations, respectively:

$$\rho_0 \frac{\partial u_i}{\partial x_i} = \dot{s}_G, \quad (1)$$

$$\frac{\partial u_i}{\partial t} + \frac{\partial (u_j u_i)}{\partial x_j} = -\frac{\partial p}{\partial x_i} + \frac{\partial \tau_{ij}}{\partial x_j} + \frac{\rho_m - \rho_0}{\rho_0} g_i, \quad (2)$$

$$\frac{\partial c_F}{\partial t} + \frac{\partial (u_i c_F)}{\partial x_i} = D_F \frac{\partial^2 c_F}{\partial x_i^2}, \quad (3)$$

$$\frac{\partial c_H}{\partial t} + \frac{\partial (u_i c_H)}{\partial x_i} = D_H \frac{\partial^2 c_H}{\partial x_i^2} + \dot{s}_{cH}. \quad (4)$$

The velocity components u_i , kinematic pressure p , food concentration c_F , and H^+ concentration c_H are the main variables to be solved. ρ_0 , ρ_m , D_F , D_H , g_i , and τ_{ij} represent the water density, mixture density, diffusivity of the food species, H^+ diffusivity, gravity acceleration rate, and viscous stress tensor, respectively. \dot{s}_G is the source term due to the secretion of gastric juice, while \dot{s}_{cH} is the source term resulting from the increase of H^+ in the secreted gastric juice. Gastric juice, an acidic digestive fluid, is secreted from the upper wall of the stomach. For healthy individuals, the intragastric pH ranges between 1.3 and 2.5, which can increase to the range of 4.5–5.8 after eating.³¹ The secretion rate of gastric juice may increase from 10 to 50 ml min⁻¹ after food intake.³² In this study, the initial pH in the stomach is 5.6, and the secretion rate of gastric juice is $2.7 \times 10^{-7} \text{ m}^3 \text{ s}^{-1}$,

$$\rho_m = (1 - c_F) \rho_0 + c_F \rho_F, \quad (5)$$

$$\nu_m = (1 - c_F) \nu_0 + c_F \nu_F. \quad (6)$$

Here, ρ_F is the density of the food. ν_m , ν_0 , and ν_F are the kinematic viscosity of the mixture, water, and food, respectively. The viscous stress tensor is calculated as

$$\tau_{ij} = 2\nu_m s_{ij}, \quad (7)$$

and the strain rate is $s_{ij} = \frac{1}{2} \left(\frac{\partial u_i}{\partial x_j} + \frac{\partial u_j}{\partial x_i} \right)$.

C. Numerical methods

A finite volume method (FVM) is used to solve the aforementioned governing equations. The solver is developed based on the open-source CFD program OpenFOAM 18.06. The solutions are advanced in time using a second-order implicit-backward method. To compute the velocity derivatives, the variables at the interfaces of the grid cells are obtained through linear interpolation. This interpolation of the interfacial values yields a second-order central difference scheme for spatial discretization. The pressure at the new time level is determined using the Poisson equation. The velocity is corrected with the pressure-implicit with splitting of operators (PISO) pressure velocity coupling scheme. The default convergence criteria in OpenFOAM are adopted in this work: The residue tolerance value for pressure is set to 10^{-6} , while 10^{-8} is used for other variables. The maximum local Courant number Co_{\max} is set to 0.2 to capture the transient motions, which have small time scales.

D. Boundary and initial conditions

The pylorus is assumed to be fully opened and static, which is a reasonable approximation for the emptying of water-like gastric contents.¹⁵ No-slip and no-penetration boundary conditions are applied to the stomach wall. The open boundary condition on the outlet (pylorus) allows a small amount of inflow and outflow to maintain mass conservation. The inflow values for species, including H^+ and food bolus, are set to 0. The velocity, pressure, and H^+ are assumed to be uniformly distributed in the initial field. A food bolus is located either in the proximal or distal stomach. [Table I](#) shows the typical boundary conditions from OpenFOAM and initial values for the simulations.

E. Computational mesh

The computational meshes were generated by ANSYS ICEM 19.2; mesh 1 is used to illustrate the mesh features (mesh 2 is finer but has a similar pattern of cell distribution), as shown in [Fig. 2](#). Four prism layers have been created from the triangulated surface mesh. The majority volume of the interior is filled with hexahedral cells, tetrahedral cells are used as transitions between them, and pyramids are

TABLE I. Boundary and initial conditions of simulations.

Field	Wall	Outlet	Initial value
$u_i(\text{m s}^{-1})$	movingWallVelocity	pressureInletOutletVelocity	0
$p'(\text{m}^2 \text{s}^{-2})^a$	fixedFluxPressure	totalPressure	0
$c_H(\text{mol L}^{-1})$	zeroGradient	inletOutlet	2.5×10^{-6}
$c_F(-)$	zeroGradient	inletOutlet	Non-uniform

^aThe alternative pressure, $p' = p - \rho g x_2$.

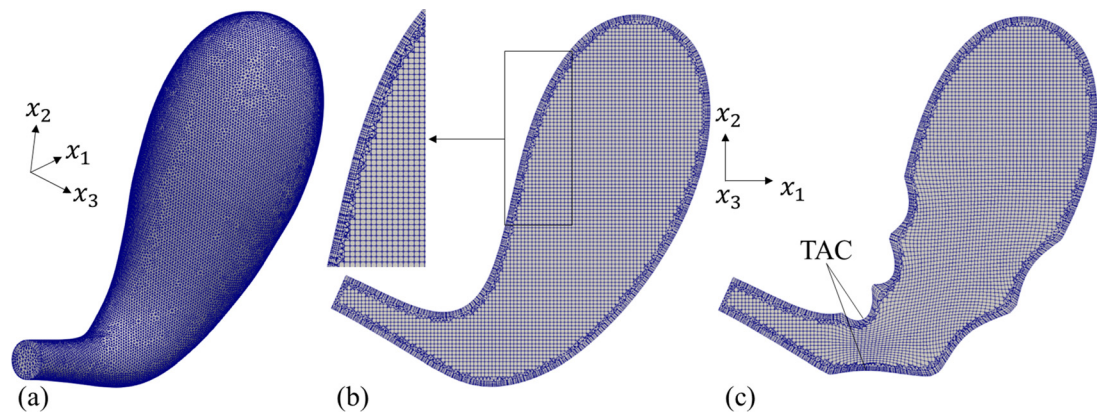


FIG. 2. View of the computational mesh, which has 602 547 cells. (a) Surface mesh, (b) cross-sectional view of the initial mesh and zoomed view of the left part, (c) the mesh in the cross section when a TAC is at its most occluded state.

TABLE II. Cell numbers of different types in the meshes 1 and 2.

Type	Hexahedra	Prisms	Pyramids	Tetrahedra	In total
Number of the mesh 1	101 383	209 112	19 144	272 908	602 547
Number of the mesh 2	663 268	689 420	66 600	926 450	2 345 738

used to ensure conformity between tetrahedral and hexahedral quad faces. The overall number of cells for each type is shown in Table II.

Cell orthogonality, skewness, and aspect ratio are commonly used metrics to assess mesh quality.³³ The results of the mesh checks at different times are listed in Table III. In OpenFOAM, a maximum face non-orthogonality angle below 70° is considered safe. Generally, a

maximum skewness value up to 0.95 is acceptable, and the threshold in OpenFOAM is 4. The maximum aspect ratio should be maintained below 35, and the threshold in OpenFOAM is 1000. It can be seen that the mesh quality meets the computational requirements well, and there are no cells significantly distorted even with remarkable deformation of the geometry during the calculation [see Fig. 2(c)]. Consequently, good mesh quality is guaranteed throughout the computations, enabling high accuracy simulations.

III. DESCRIPTION OF TEST CASES

The stomach is initially filled with water and one food bolus. The food bolus is assumed to be a collection of unlinked small food particles, which will be rapidly dispersed and mixed by the ambient fluid, rather than a single coherent body. This assumption is reasonably supported by Sicard *et al.*,²⁷ therefore, the food bolus is a soluble species. To highlight the functional difference between the distal and proximal stomach, the food bolus is initially located either in the distal or proximal region, as shown in Fig. 3. In order to study the interaction between the bolus and gastric flow under different gravity conditions, a density ratio of $\rho_F/\rho_0 = 1.1$ is considered. The viscosity of the bolus

TABLE III. Results of mesh quality check for mesh 1 at different times.

Quality metrics		Non-orthogonality (°)	Skewness	Aspect ratio
Maximum value	$t = 0 \text{ s}$	60	0.83	7.8
	$t = 60 \text{ s}^a$	68	0.88	9.1
	$t = 120 \text{ s}^a$	68	0.88	9.3
	$t = 180 \text{ s}^a$	68	0.88	9.3
	$t = 1800 \text{ s}^b$	68	0.89	9.1

^aTACs are considered in the simulation.
^bTACs are not considered in the simulation.

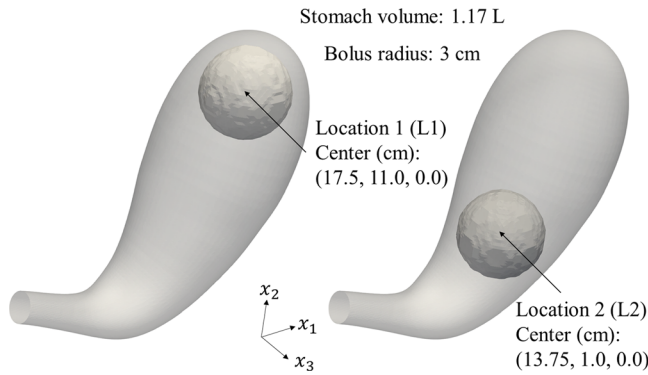


FIG. 3. The initial distribution of the food bolus (located at the location 1 or 2) inside the stomach, which has a spherical shape with a radius of 3 cm. Locations 1 and 2 are on the stomach axis [see Fig. 1(b), white dashed line], and their center coordinates (in centimeters) are (17.5, 11.0, 0.0) and (13.75, 1.0, 0.0), respectively. The space around the food bolus is filled with water at $t = 0$ s. The overall capacity of the stomach is 1.17 L.

is assumed to be $1.0 \times 10^{-5} \text{ m}^2 \text{ s}^{-1}$ ($1.1 \times 10^{-2} \text{ Pa s}$); however, it is worth noting that real foods exhibit viscosities that range from values comparable to that of water ($\sim 1.0 \times 10^{-3} \text{ Pa s}$) to as high as 10 Pa s .³⁴ The density of real gastric juice is close to that of water, while its viscosity ranges from 1.0×10^{-2} to 2.0 Pa s due to the presence of mucins and pepsins.³¹ The gastric juice in this study is assumed to have the same density and viscosity as water, without considering the contained mucins and pepsins. The physical properties of the food, gastric juice, and water are provided in Table IV. We consider zero gravity (0G, in a satellite or space vehicle where a zero gravity environment may occur), half gravity (0.5G, given tentatively to represent a reduced gravity environment), and Earth's gravity (1G) conditions. Under the 0G condition, the food is initially positioned at locations “L1” (proximal stomach) or “L2” (distal stomach) to explore the dynamics at different stages of digestion. However, under nonzero gravity conditions, only the initial location L1 is considered because the food rapidly falls from L1 to L2 when gravity is present. Mesh independence analysis and qualitative comparison with previous studies can be found in

TABLE IV. The properties of the food, gastric juice, and water.

Species	Density (kg m^{-3})	Viscosity ($\text{m}^2 \text{ s}^{-1}$)	Diffusivity ($\text{m}^2 \text{ s}^{-1}$)
Food	ρ_F , ³⁵ 1100	ν_F , 1.0×10^{-5}	D_F , ³⁶ 3.09×10^{-9}
Gastric juice	1000	1.0×10^{-6}	D_H , ³⁷ 3.3×10^{-9}
Water	ρ_0 , 1000	ν_0 , 1.0×10^{-6}	...

Appendix B. The direction of gravity is oriented opposite to the x_2 -axis, aligning with a common configuration relative to stomach geometry. A common orientation is focused in the study. However, an exploration of the effects of stomach orientation on gastric emptying dynamics is given in Appendix C.

IV. RESULTS AND DISCUSSION

A. Effects of gravity on food retention

We define the retention rate of the food bolus as $r_{gr} = \frac{V_F}{V_{F0}}$, where V_F is the volume of the food in the stomach, given by $V_F = \int_V c_F dV$. V_{F0} is the initial volume of the food. The global retention rate of the food bolus is depicted in Fig. 4(a). Under the 0.5G or 1G conditions, the food leaves the stomach rapidly, while there is a lag time of emptying under the 0G condition. This emptying lag is particularly evident when the food bolus is initially located at the position L1 in the proximal stomach (the case 0GL1). In this scenario, the food is almost undischarged in the first 6 min. However, after the lag time, the food is quickly emptied. On the other hand, when the food bolus is initially located at the position L2, it is emptied more rapidly and experiences a shorter lag time compared to the food bolus at L1. This is attributed to the shorter distance between the food bolus at L2 and the pylorus, as well as the stronger flow dynamics in the distal stomach.

In the 0.5G and 1G cases, the rapid decrease in the food retention rate r_{gr} can be identified. This is due to the decrease in stomach volume as a result of ACWs starting from a quiescent state (the first ACW initiates at 0 s, the second ACW starts at 20 s, and the stomach volume reaches a minimum value at approximately 39 s). In addition, the fast emptying of foods in the first several minutes is also related to the

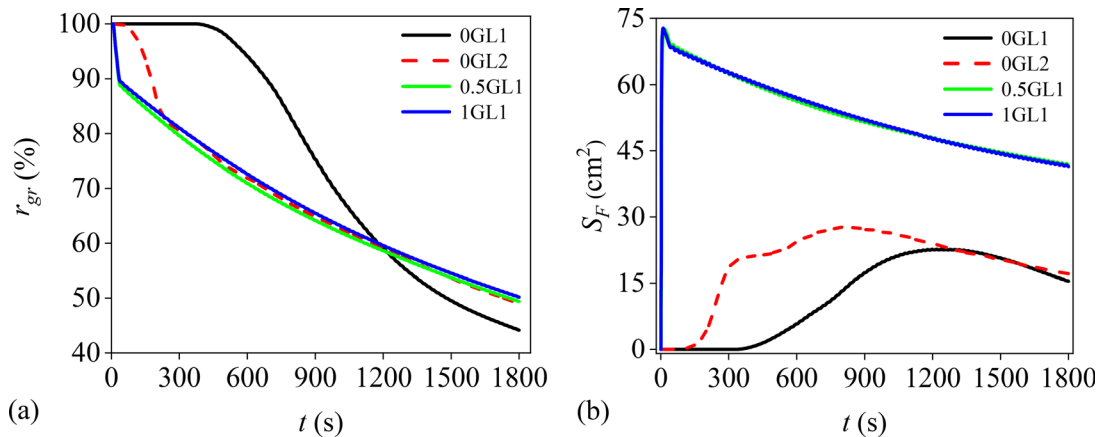


FIG. 4. (a) The retention rate of the food in the stomach (r_{gr}) and (b) the food on the stomach wall ($S_F = \int_S c_F dS$, integral of the food on the gastric wall).

small volume fraction of food, nonzero gravity, and an open pylorus. Gravity drives the food bolus of higher density (compared to water) to access the pylorus faster. This fast-emptying phenomenon is qualitatively comparable with previous *in vivo* and *in silico* studies. The *in vivo* study by Tougas *et al.*²⁴ also demonstrated that transpyloric flow was occurring and was especially rapid just before lumen occlusion by antropyloroduodenal contractions when the pylorus was open. An *in silico* study showed that over 50% content (water) was emptied within 150 s.¹⁵ This rapid drop in food retention, however, does not occur in 0G cases.

After this fast-emptying process in the early stage, r_{gr} changes almost linearly with time, indicating a nearly constant emptying rate. The food is emptied slightly slower in the case of 1GL1 compared to the case of 0.5GL1. However, after around 200 s, the r_{gr} profiles in the cases 0GL2, 0.5GL1, and 1GL1 become very similar. After about 1200 s, the r_{gr} value in the case 0GL1 becomes lower than those in the other cases.

Figure 4(b) compares the weighted food fraction (S_F , cm²) on the stomach wall in different cases. S_F indicates the amount of food in contact with the inner surface of the stomach wall. This contact can influence the adhesion of gastric objects to the gastric mucosa, thereby prolonging their retention, as observed in an *in vitro* experiment.³⁸ S_F increases rapidly in cases with nonzero gravity, reaching its maximum

value at around 10 s. Subsequently, due to the gastric emptying, S_F starts to decrease at 10 s. The S_F history changes only marginally when gravity increases from 0.5G to 1G. In the 0G cases, S_F slowly increases until 1100 s (case 0GL1) or 800 s (case 0GL2), then gradually decreases. During the emptying process, S_F in the 0G cases remains lower than its values in the 0.5G and 1G cases, indicating that the absence of gravity reduces the likelihood of gastric objects adhering to the stomach wall. Gravity aids the settling of gastric contents toward the lower stomach, such as the antrum and pylorus, increasing the likelihood of food particles adhering to the stomach walls, especially along the bottom or greater curvature. In contrast, under zero gravity conditions, the absence of gravitational force prevents this natural settling, causing the food to remain suspended within the gastric fluid and distribute more evenly. This reduces their contact with the stomach walls. The peristaltic movements, which mix and propel contents, become dominant under the zero gravity condition, keeping the food in constant motion and further decreasing their likelihood of adhesion.

The food distributions at different time instances are shown in Fig. 5. The different distributions of the food suggest that variations in gravity magnitude results in different hydrodynamics and transport of food species in the stomach. The emptying of food in the proximal stomach is notably slower compared to the rapid emptying observed in the distal stomach. This finding aligns with the study by Anvari

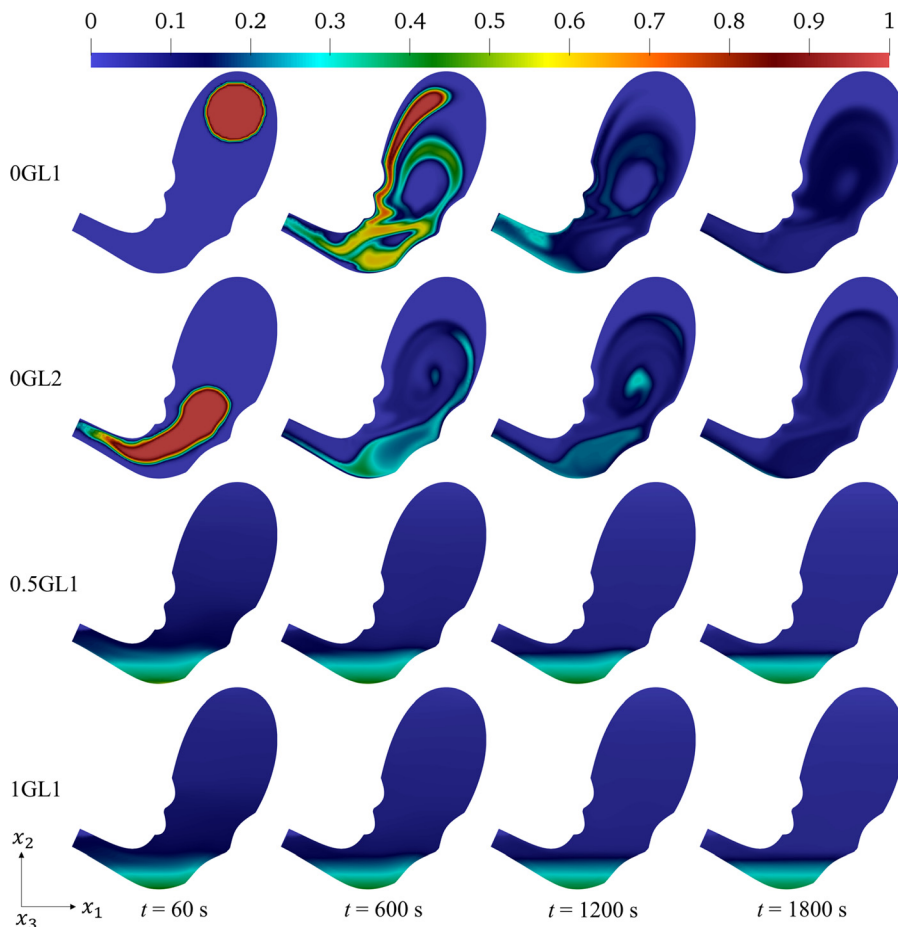


FIG. 5. Time-dependent food distributions (volume fraction) in the cross-plane of the stomach. The boundary of the food is tracked by tracking concentration gradients, visualized using color gradients, where red indicates higher concentrations of food particles, distinguishing them from lower concentration or water-dominated areas.

et al.,³⁹ which indicated that the effect of gravity on gastric emptying may stem from changes in intragastric distribution.

As can be seen in the 0.5G and 1G cases, the food settles to the bottom of the stomach in a short time. This is in line with our previous study,²¹ which shows that the heavy food particles settle down to the distal stomach within a few seconds. The distribution of food is similar in 0.5GL1 and 1GL1 cases. Notably, the volume fraction of the deposited food has a smaller value in the upper layer, as seen in 0.5GL1 and 1GL1 in Fig. 5, which suggests that the heavy food near the upper layer (close to the lesser curvature) is emptied more rapidly. Additionally, the distribution of the deposited food undergoes minimal changes over time, indicating the poor mixing effects on the heavier food (compared with water). However, it should be noted that there is evidence of gastric motor dysfunction under microgravity conditions, which results in weakened gastric motility.⁴⁰ This reduction in motility may adversely affect the efficiency of gastric mixing. Moreover, for foods comprising particles of diverse sizes and densities, the absence of gravitational forces to facilitate their stratification and movement could lead to sub-optimal mixing.

It can be seen in Fig. 5 that the food bolus at location L1 is still suspended in the stomach under the 0G condition at $t = 60$ s. In contrast, the food bolus at location L2 is more efficiently mixed with the

water; the food bolus is stretched and transported to the pylorus due to the effects of ACWs. This observation confirms the poor mixing effects in the fundus, which is in line with the simulation findings of Harrison *et al.*,¹⁵ who suggested that the top stomach has limited mixing effects on the gastric content. In cases 0GL1 and 0GL2, the food that contacts the stomach wall changes over time. Conversely, in cases 0.5GL1 and 1GL1, the food that contacts the stomach wall remains stable near the stomach bottom. These findings are consistent with the statistic results presented in Fig. 4(b). When the gravity is not zero, the increase in its magnitude has only a marginal influence on the emptying and distribution of the food species.

B. Effects of gravity magnitude on pH distribution

The concentration of H^+ in gastric juice determines the pH distribution in gastric contents, playing an important role in the activity of enzymes. The pH distributions at various times are displayed in Fig. 6. At the same time instance, the results of the cases 0GL1 and 0GL2 show a similar pattern. Under the 0G condition, the pH is lower in the antrum region and exhibits a local minimum near the fundus center.

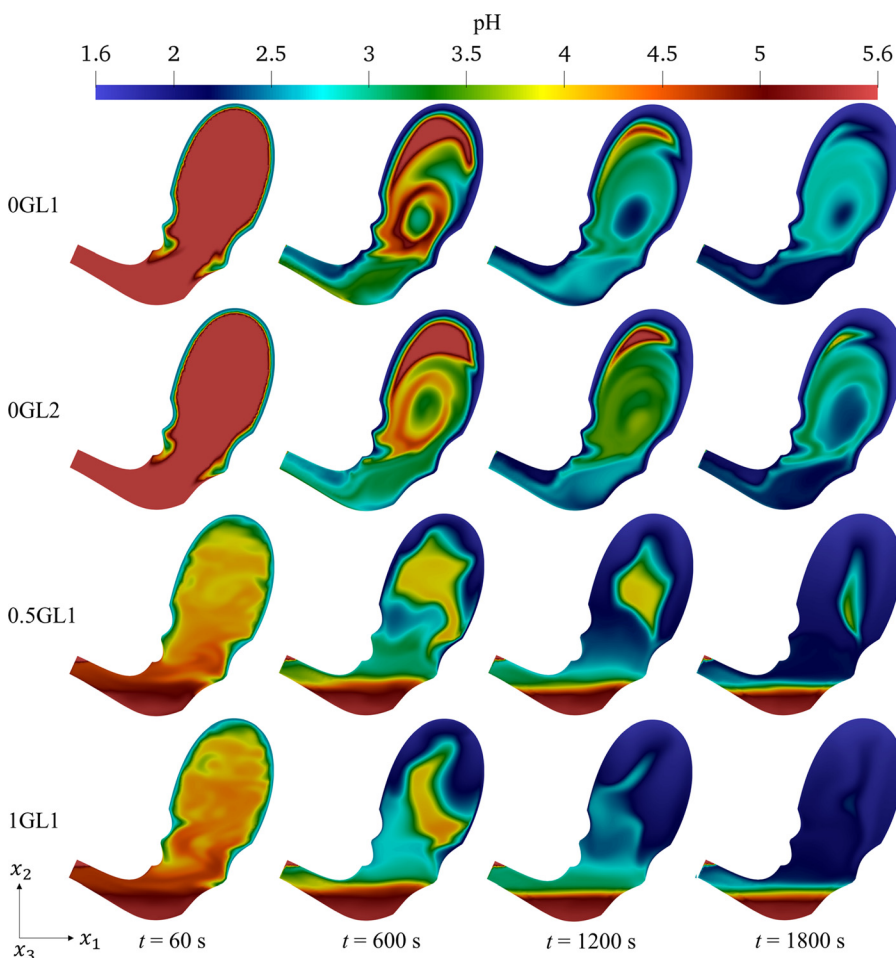


FIG. 6. pH distributions at different times in the cross-plane of the stomach.

The cases 0.5GL1 and 1GL1 also show a similar pattern. The distribution of pH is influenced by the food distribution, as the transport of H^+ in foods encounters higher flow resistance due to the high viscosity of the food. The proximal stomach has lower pH values under the 0.5G or 1G conditions compared to the 0G condition. This suggests that gravity facilitates the transport of H^+ to the proximal stomach. The deposition of the food at the stomach bottom increases the

outflow resistance, narrowing the passage for outflow. When antral contractions occur, H^+ are pushed upward. Under the 0.5G and 1G conditions, the pH level in the bottom region is high, indicating that it is difficult for H^+ to penetrate into the food near the stomach bottom.

It should be noted that the viscosity of digesta made of solid foods may be several hundred times higher than that of water. As a result, the transport of H^+ in solid foods is much slower, and the

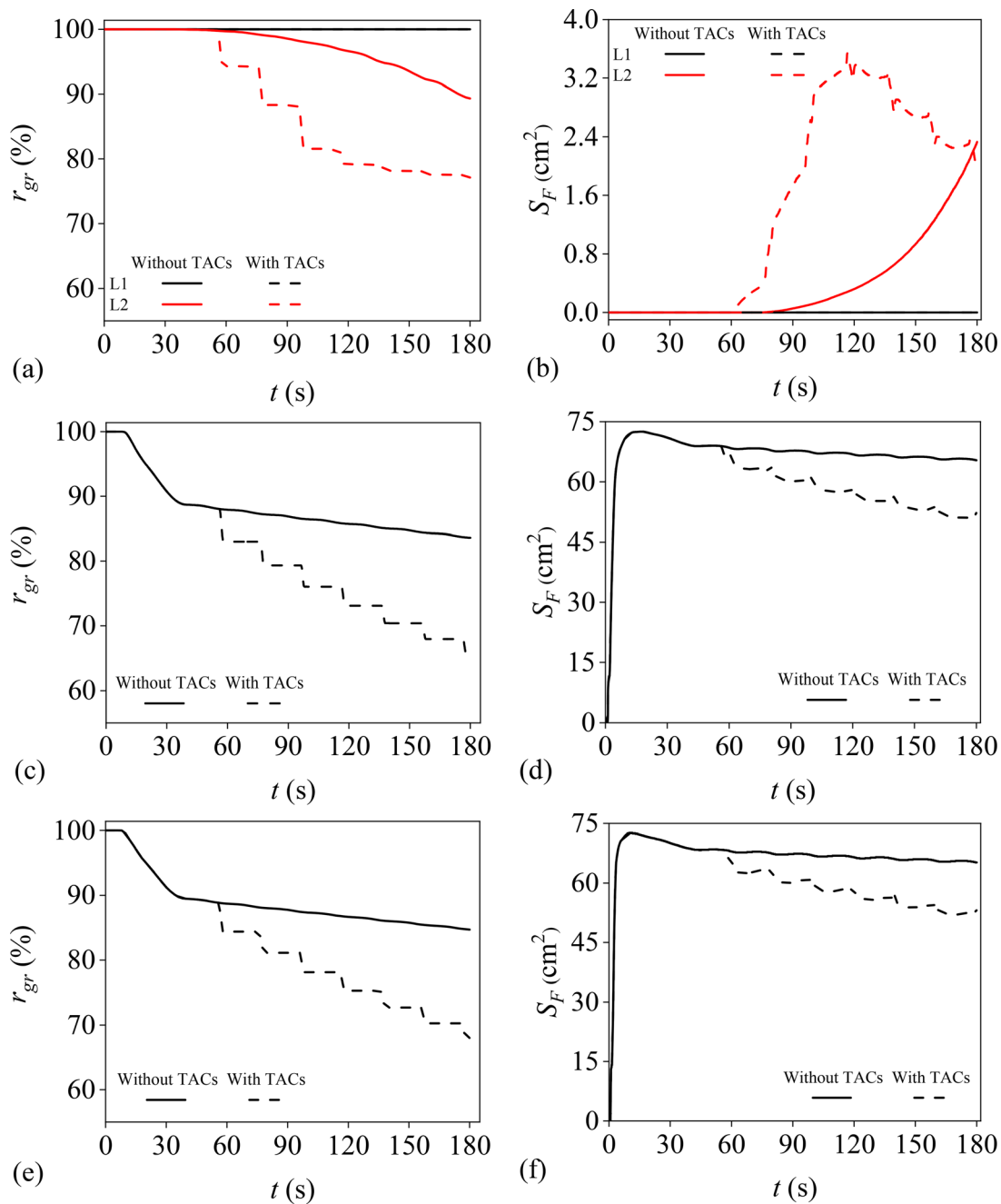


FIG. 7. Effects of TACs on gastric retention rate (r_{gr}): (a) 0G, (c) 0.5GL1, and (e) 1GL1; and weighted food fraction (S_F): (b) 0G, (d) 0.5GL1, and (f) 1GL1.

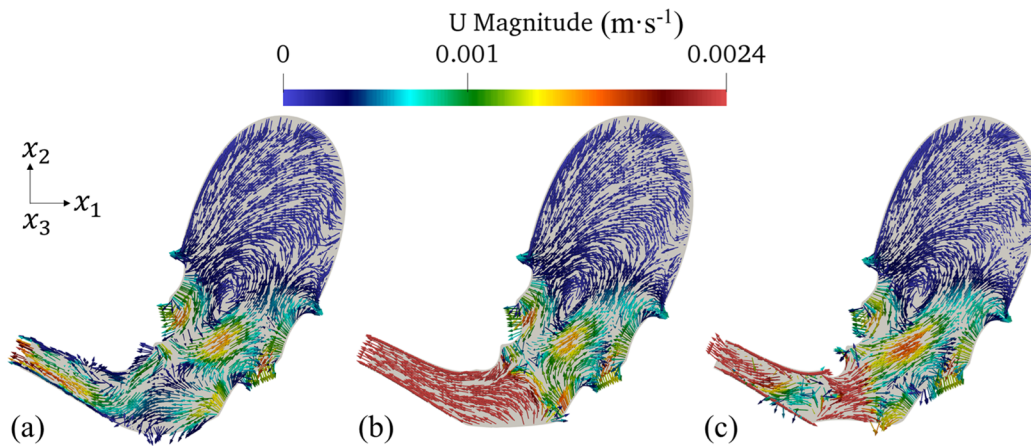


FIG. 8. Representative velocity vectors in the cross section during the contraction process of the first TAC, 0GL1: (a) $t = 56$ s, $|u|_{\max} = 2.39 \times 10^{-3} \text{ m s}^{-1}$; (b) $t = 57$ s, $|u|_{\max} = 9.14 \times 10^{-2} \text{ m s}^{-1}$; and (c) $t = 58$ s, $|u|_{\max} = 1.83 \times 10^{-2} \text{ m s}^{-1}$.

corresponding pH distribution can be significantly different from the findings of this study.

C. Effects of TACs under different gravity conditions

We have examined the effects of TACs under different gravity conditions within the first 3 min. The TAC starts at 56 s, lasts for 4 s, and repeats every 20 s. In the 0G condition, TACs have almost no effects on the gastric retention rate r_{gr} and the inner-surface food concentration S_F when the food bolus is originally placed at location L1 (in the proximal stomach). However, the emptying and food concentration at the stomach's inner surface are accelerated by TACs when the food is originally placed at location L2 (in the distal stomach), as seen in Figs. 7(a) and 7(b) for comparison. Under the 0.5G and 1G conditions, the food emptying is considerably enhanced during a TAC period, as shown in Figs. 7(c) and 7(e). Figures 7(d) and 7(f) also show that S_F is lower when TACs are taken into account. This is partly due to the fact that TACs accelerate the emptying of food.

Figures 8 and 9 demonstrate the velocity fields obtained from the CFD simulations of cases 0GL1 and 1GL1, respectively. The flow fields in a cross-sectional plane of the stomach are shown. The TAC starts at 56 s and approaches the most occluded situation at 58 s. The results show that the strongest fluid motions exist in the antropyloric region, while relatively slow recirculation appears between the distal and proximal stomach regions. With the pyloric sphincter being open, the TAC significantly increases the outflow rate, resulting in a higher emptying rate.

At the same time, the maximum velocity magnitude in case 0GL1 is smaller than that in case 1GL1. In the 1G case, a region of high velocity magnitude is found close to the lesser curvature and the pylorus at $t = 56$ s. The velocity near the greater curvature of the stomach is lower, due to the higher viscosity of the food that deposits on the greater curvature (as seen in previous results of 1GL1 in Fig. 5), which creates higher resistance to the flow in that region. At $t = 57$ s, the flow close to the pylorus region is more intensive and consistently aligned in a direction toward the exit. At $t = 58$ s, the TAC reaches its peak

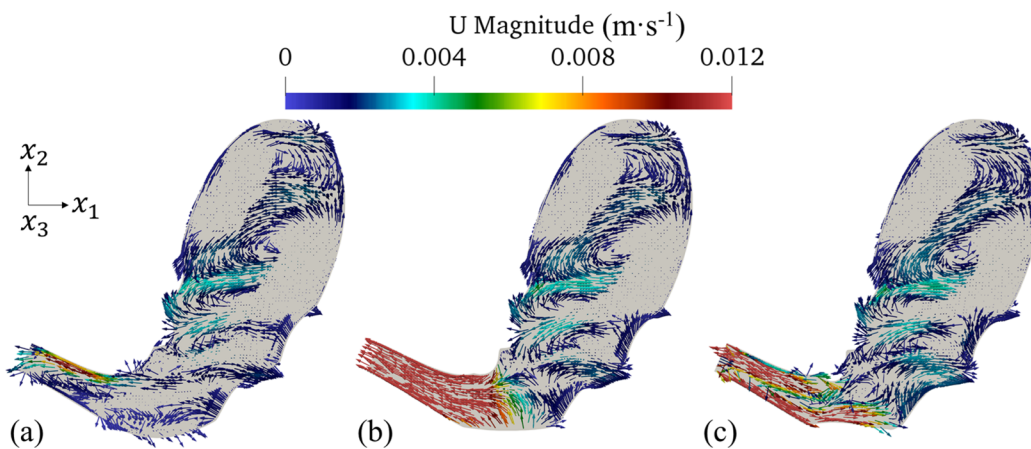


FIG. 9. Representative velocity vectors in the cross section during the contraction process of the first TAC, 1GL1: (a) $t = 56$ s, $|u|_{\max} = 1.20 \times 10^{-2} \text{ m s}^{-1}$; (b) $t = 57$ s, $|u|_{\max} = 9.97 \times 10^{-2} \text{ m s}^{-1}$; and (c) $t = 58$ s, $|u|_{\max} = 2.99 \times 10^{-2} \text{ m s}^{-1}$.

contraction, causing some fluids to be pushed back into the stomach lumen. This retropulsive flow is strong, with a speed many times faster than that of the TAC. However, the flow away from the TAC is relatively weak. The flow in the proximal stomach is only marginally affected by the contraction, which explains why the food is retained for a longer time when it is located in the proximal stomach (see Fig. 5). Flow recirculation can be observed between two continuous ACWs and in the region above the ACWs.

Wall shear stress (WSS) is one of the most frequently studied parameters in the pulsatile flows.⁴¹ In the context of gastric dynamics, WSS at the inner surface of the stomach plays a crucial role. The WSS generated by gastric flows is defined as

$$\text{WSS} = \left| \rho_m \nu_m n_j \frac{\partial u_i}{\partial x_j} \right|, \quad (8)$$

where n_j represents the direction normal to the inner surface of the stomach. WSS is directly influenced by the dynamic viscosity of the gastric contents and the velocity gradient. Therefore, understanding the distribution and variation of WSS provides valuable insights into the complex flow dynamics within the gastric system.

The contour map of WSS shown in Figs. 10 and 11 provides a comprehensive visualization of the spatial distribution of this important parameter at the inner stomach surface. In particular, the antropyloric region and the contraction region are characterized by higher values of WSS due to the strong flow dynamics in these areas. The localized high WSS regions can be attributed to the strong mechanical forces exerted by the fluid flow on the stomach walls. Comparing the 0G and 1G cases at a specific time instance ($t = 56$ s), it can be seen that the maximum WSS value is higher in the latter case. This observation can be attributed to the influence of gravity, which contributes to the enhancement of flow dynamics and consequently leads to increased shear forces acting on the stomach walls. Furthermore, the TAC significantly enlarges the high WSS area, especially in the antrum region. The TAC-induced contractile motions of the stomach walls intensify the flow and result in heightened WSS values, indicating

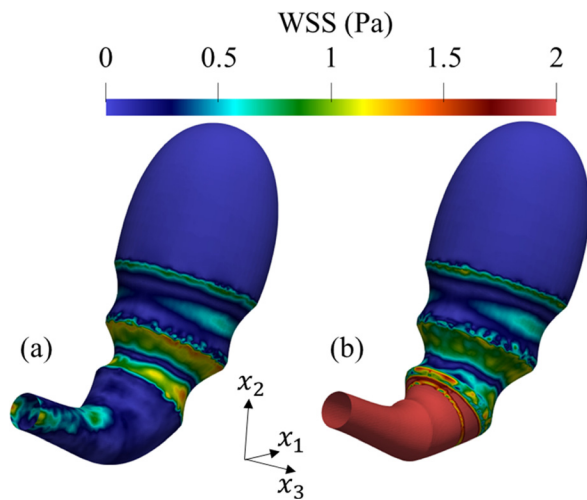


FIG. 10. Wall shear stress (WSS) of 0GL1: (a) $t = 56$ s, $|\text{WSS}|_{\max} = 2.04$ Pa and (b) $t = 57$ s, $|\text{WSS}|_{\max} = 93.6$ Pa.

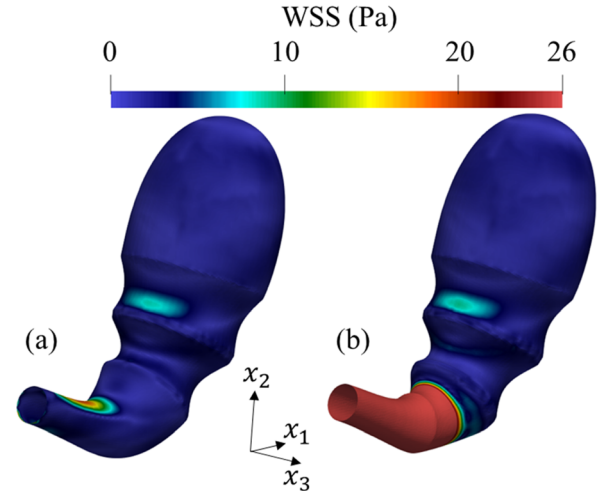


FIG. 11. Wall shear stress (WSS) of 1GL1: (a) $t = 56$ s, $|\text{WSS}|_{\max} = 26.2$ Pa and (b) $t = 57$ s, $|\text{WSS}|_{\max} = 1780$ Pa.

enhanced mechanical stimuli experienced by the gastric inner surface. Interestingly, the upper stomach surface experiences much lower WSS as the wall movements have only a marginal effect in this region. As the dominant flow dynamics occur in the antropyloric region and the contraction region, the upper surface experiences relatively subdued mechanical forces, leading to reduced WSS values.

To gain a comprehensive understanding of the temporal evolution of WSS, the history of the surface-averaged WSS ($\overline{\text{WSS}} = \frac{\int_s \text{WSS} ds}{\int_s ds}$, Pa) is examined and shown in Fig. 12. The analysis shows a significant increase in $\overline{\text{WSS}}$ during the onset of the TAC, followed by a decline over time. This behavior suggests that the mechanical stimuli experienced by the stomach walls, as represented by $\overline{\text{WSS}}$, are augmented during TACs but gradually diminish as the

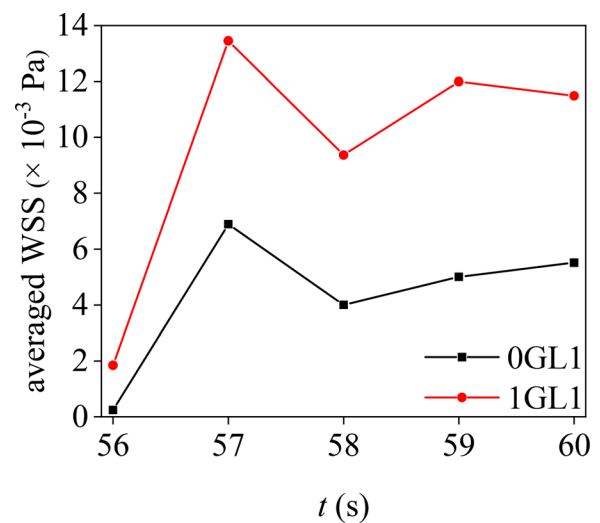


FIG. 12. Comparisons of $\overline{\text{WSS}}$ over the stomach wall at 0G and 1G conditions.

contractions subside. Interestingly, a similar trend is observed in both the 0GL1 and 1GL1 cases, implying that the influence of TACs on \overline{WSS} is independent of the gravity condition. Nevertheless, it should be noted that the absolute values of \overline{WSS} are higher under the 1G condition compared to the 0G condition, indicating the important role of gravity in modulating the magnitude of \overline{WSS} in the stomach.

V. CONCLUSION

A CFD study has been carried out to compare the digestion processes in the human stomach under normal gravity (1G) and reduced gravity (0.5G and 0G) conditions. In the presence of gravity, the food rapidly settles down into the antrum within a short period of time. When the food is initially located in the proximal stomach under the 0G condition, the emptying of the food is delayed by about 6 min. The food concentration on the inner surface of the stomach is apparently reduced when the gravity is reduced from 1G to 0G. When gravity is present, the magnitude of gravity and the initial location of the food do not significantly affect the food concentration.

The intragastric distribution of food and pH shows significant differences when the gravity condition varies. However, the distribution changes only slightly when the gravity changes from 0.5G to 1G. Under the 0G condition, the food floats in the stomach, while H^+ are transported to the antrum, leading to low pH values near the pylorus. In contrast, in the presence of gravity, the food deposits in the distal stomach in a short time, resulting in lower pH values in the body and fundus regions. TACs have marginal effects on food mixing in the proximal stomach, regardless of gravity's presence. Nevertheless, TACs accelerate the emptying process by up to 20% under the 0G condition after the food enters the antral region. In comparison, under the 1G condition, TACs stimulate stronger mixing and higher shear forces in the antrum and pyloric region.

Our CFD study provides qualitative insights into the effects of gravity on gastric mixing and emptying, marking an initial step toward understanding the digestion under reduced gravity. To perform a more accurate quantitative study, the CFD model should be further improved in the following aspects: An important task is to consider the real rheology of non-Newtonian gastric contents. The transport of highly viscous gastric contents may be very different from that of the water-like fluids that are typically studied. For this purpose, the disintegration models of solid foods should be coupled with the current CFD techniques. In addition, the dynamics of the pylorus should also be accounted for to make the simulated gastric emptying process more realistic.

ACKNOWLEDGMENTS

The authors gratefully acknowledged the support by the China Scholarship Council (CSC) and the Scientific Research Funds of Huaqiao University (No. 23BS108).

NOMENCLATURE

Roman symbols

A_{ACW}	Amplitude of ACWs (m)
A_{TAC}	Amplitude of TACs (m)
c_F	Volume fraction of the food (-)
c_H	Mole concentration of H^+ (kmol m^{-3})
Co_{\max}	Maximum local Courant number (-)

D_F	Diffusion coefficient of the food ($\text{m}^2 \text{s}^{-1}$)
D_H	Diffusion coefficient of H^+ ($\text{m}^2 \text{s}^{-1}$)
D_{sc}	Distance vectors from points on centerline to points on the stomach wall (m)
d_{AC}	Displacement of antral contractions (including ACWs and TACs) (m)
g_i	Gravitational acceleration (m s^{-2})
h_{ACW}	Width of ACWs (m)
l_{10}	Arc length on the centerline from the center point of the contraction to another point of the contraction (m)
\mathbf{n}	Direction vector (-)
\mathbf{n}_j	Direction normal to the inner surface of the stomach (-)
p	Static pressure divided by density ($\text{m}^2 \text{s}^{-2}$)
p'	Alternative pressure ($\text{m}^2 \text{s}^{-2}$)
r_{gr}	Gastric retention rate of the food (-)
S_F	Integral of the food on the inner wall of the stomach (m^2)
s_{ij}	Strain rate (s^{-1})
\dot{s}_{cH}	Source term of H^+ ($\text{kmol m}^{-3} \text{s}^{-1}$)
\dot{s}_G	Source term due to secretion of gastric juice ($\text{kg m}^{-3} \text{s}^{-1}$)
T_{ACW}^{lc}	Life cycle of ACWs (s)
T_{TAC}^{lc}	Life cycle of TACs (s)
t	Time (s)
t_0^{ACW}	Start time of ACWs (s)
t_0^{TAC}	Start time of TACs (s)
u_{ACW}	Speed of ACWs (m s^{-1})
u_i	Velocity component (m s^{-1})
u_j	Velocity component (m s^{-1})
V_F	Volume of the food in the stomach (m^3)
V_{F0}	Initial value of V_F (m^3)

Greek symbols

ρ_F	Density of the food (kg m^{-3})
ρ_m	Density of the mixture (kg m^{-3})
ρ_0	Density of the water (kg m^{-3})
τ_{ij}	Viscous stress tensor ($\text{m}^2 \text{s}^{-2}$)
ν_F	Kinematic viscosity of the food ($\text{m}^2 \text{s}^{-1}$)
ν_m	Kinematic viscosity of the mixture ($\text{m}^2 \text{s}^{-1}$)

Acronyms

2D	Two-dimensional
3D	Three-dimensional
ACWs	Antral contraction waves
B-SPH	Biomechanical-smoothed particle hydrodynamics
CFD	Computational fluid dynamics
FVM	Finite volume method
PISO	Pressure-implicit with splitting of operators
SAS	Space adaptation syndrome
TACs	Terminal antral contractions
WSS	Wall shear stress
\overline{WSS}	Averaged WSS

AUTHOR DECLARATIONS

Conflict of Interest

The authors have no conflicts to disclose.

Author Contributions

Changyong Li: Conceptualization (equal); Formal analysis (equal); Funding acquisition (lead); Investigation (lead); Methodology (equal); Software (lead); Validation (equal); Writing – original draft (lead); Writing – review & editing (equal). **Xiao Dong Chen:** Conceptualization (equal); Project administration (equal); Supervision (equal); Writing – review & editing (equal). **Jie Xiao:** Supervision (equal); Writing – review & editing (equal). **Renpan Deng:** Writing – review & editing (equal). **Yan Jin:** Formal analysis (equal); Methodology (equal); Project administration (equal); Supervision (equal); Validation (equal); Writing – review & editing (equal).

DATA AVAILABILITY

The data that support the findings of this study are available from the corresponding authors upon reasonable request.

APPENDIX A: DESCRIPTIONS OF GEOMETRIC PARAMETERS, COMPUTATIONAL PARAMETERS, AND CONTRACTION WAVES

The centerline equation [units in cm, white dashed line in Fig. 1(b)] is

$$x_2 = 0.0067x_1^3 - 0.0624x_1^2 - 0.3426x_1, \quad x_3 = 0. \quad (\text{A1})$$

The basic frame for constructing the geometry is a profile line and a series of circles with different diameters. The centerline is composed of the centers of these circles, which are perpendicular to the centerline. Then, the geometry is generated with the loft function using SOLIDWORKS® 2016. The loft feature creates a stomach shape by combining the circles and the profile line (acts as a guide line).

As shown in Fig. 1(b), point S is the center where ACW starts, and point E is the center where the ACW ends. ACW initiates every 20 s from S and ends after 60 s at E, meaning the life circle of an ACW is 60 s, so there are always 3 ACWs on the stomach at any time. The length of the curve SE (L_{SE}) is approximately 129.96 mm, so the velocity of ACWs sliding along the centerline is approximately 2.166 mm s^{-1} . The life circle of a TAC is 4 s.

The stomach motilities are represented by the following equations:

$$\mathbf{d}_{AC}(\mathbf{x}_1) = \mathbf{n} \cos\left(\frac{\pi}{2} \left\lfloor \frac{2l_{10}}{h_{ACW}} \right\rfloor_{-1,1}\right) (t_{ACW} + t_{TAC}), \quad (\text{A2})$$

$$t_{ACW} = A_{ACW} \sin\left(\pi \left\lfloor \frac{t - t_0^{ACW}}{T_{ACW}^{lc}} \right\rfloor_{0,1}\right), \quad (\text{A3})$$

$$t_{TAC} = A_{TAC} \sin\left(\pi \left\lfloor \frac{t - t_0^{TAC}}{T_{TAC}^{lc}} \right\rfloor_{0,1}\right). \quad (\text{A4})$$

Here, \mathbf{d}_{AC} is the displacement of ACW, $\mathbf{n} = \frac{\mathbf{D}_{sc}}{|\mathbf{D}_{sc}|}$ is the direction vector, \mathbf{D}_{sc} means distance vectors pointing from points on centerline to points on the stomach wall that have the smallest distance. l_{10} is the arc length on the centerline from the center point of the contraction to another point of the contraction. h_{ACW} is the ACW width (defined as the arc length of the centerline part corresponding to that ACW), which is 38 mm in our simulations. A_{ACW} and A_{TAC}

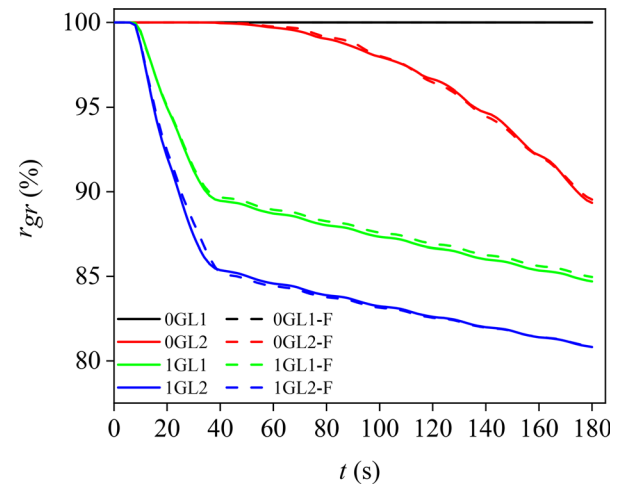


FIG. 13. The gastric retention rate (r_{gr}) is used to show the mesh sensitivity. The solid lines indicate the results from the course mesh (mesh 1, 602 547 elements) and the dash lines indicate the results from the fine mesh (mesh 2, 2 345 738 elements). The MPI (message passing interface) parallel calculations are performed with 48 processors (three nodes of a computer cluster with CPU type 2×E5-267, each node having 16 processors), and these take around 11 h with mesh 1 and 67 h with mesh 2.

are the ACW amplitude and TAC amplitude, respectively, they are both 10 mm in our simulation. T_{ACW}^{lc} and T_{TAC}^{lc} are the life circle of an ACW and a TAC, respectively. t_0^{ACW} indicates the start time of an ACW (e.g., 0 s, 20 s, 40 s, 60 s, ...). t_0^{TAC} indicates the start time of a TAC (e.g., 56 s, 76 s, 96 s, 116 s, ...). $\llbracket x \rrbracket_{a,b}$ is a function defined for a general variable x ,

$$\llbracket x \rrbracket_{a,b} = \begin{cases} x, & a \leq x \leq b, \\ 0, & x < a \text{ or } x > b. \end{cases} \quad (\text{A5})$$

Details regarding the descriptions of geometric parameters, computational parameters, and contraction waves can be also found in our previous study.²⁰

APPENDIX B: ACCURACY OF THE NUMERICAL RESULTS

1. Mesh independence analysis

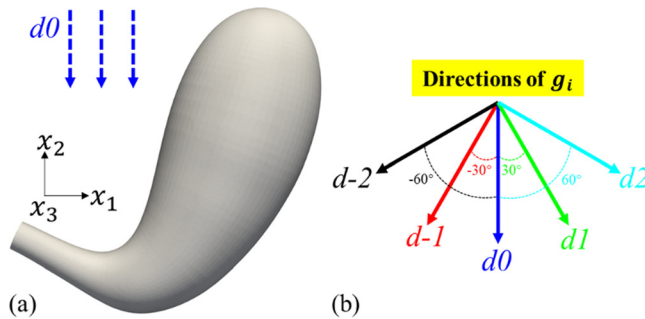
A mesh independence study has been carried out to verify that the governing equations are solved precisely. Two mesh resolutions

TABLE V. Maximum velocity in different *in silico* studies, TACs are not considered.

Dimension of geometry	Maximum velocity (mm s^{-1})	References
2D	8–10	42
2D	77.4–112.3	43
3D	78–119	13
3D	13.5–62	44
3D	19.9	1GL1 case in this study

TABLE VI. Different directions simulated in this study.

Index	-2	-1	0	1	2
Directions	$\left(-\frac{\sqrt{3}}{2}, -\frac{1}{2}, 0\right)$	$\left(-\frac{1}{2}, -\frac{\sqrt{3}}{2}, 0\right)$	$(0, -1, 0)$	$\left(\frac{1}{2}, -\frac{\sqrt{3}}{2}, 0\right)$	$\left(\frac{\sqrt{3}}{2}, -\frac{1}{2}, 0\right)$

**FIG. 14.** Diagram illustrating various stomach orientations: (a) stomach oriented in the most common direction of gravity and (b) schematic representation of variations in the direction of gravity.

(mesh 1 and mesh 2) are used to calculate the test cases described in Sec. III. The CFD simulations enable us to view and quantify food emptying in the stomach. The numerical results of the retention rate r_{gr} are compared in Fig. 13 to demonstrate the mesh convergence. As seen from Fig. 13, the retention rates are not qualitatively changed when a higher mesh resolution is used. Based on the mesh-convergence study, mesh 1 is used in our study.

2. Qualitative comparison with previous studies

Due to individual differences, complexity of gastric digestion, and simplification of our numerical model, it is difficult to find realistic and reliable data to validate our CFD results. However, it is possible to qualitatively compare our CFD results with those from

previous studies, because the physiological and geometrical parameters in our study are within the range of real values.

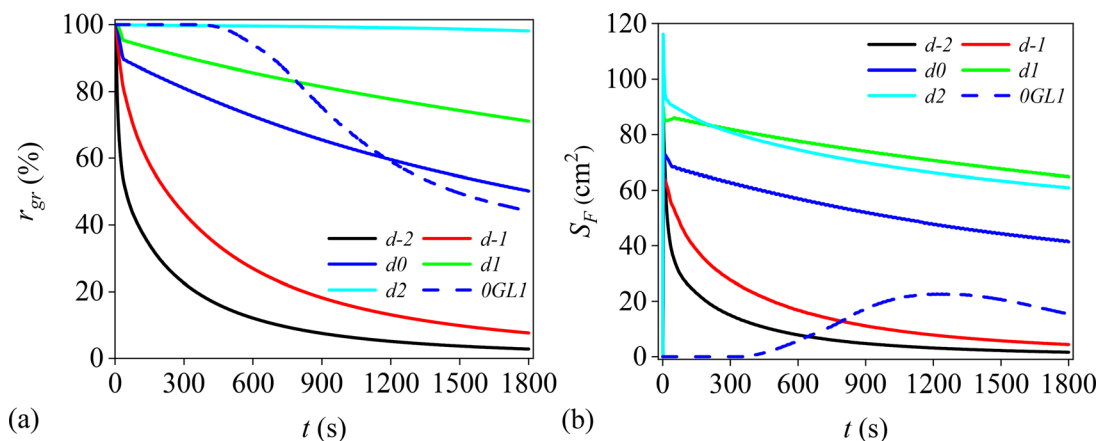
Table V shows the maximum local velocity from different CFD studies with water-like gastric contents. The maximum velocity by our model is qualitatively comparable with previous numerical studies.

In addition to the maximum velocity values, we have also compared the flow phenomena captured in our simulation with previous studies. For example, our numerical results indicate that TACs stimulate strong retropulsive flows; this is in accordance with the findings from previous studies. Despite assumptions and simplifications in our CFD model, our numerical results are qualitatively similar to those from previous studies.

APPENDIX C: EFFECTS OF STOMACH ORIENTATION ON GASTRIC EMPTYING DYNAMICS

Our initial model positioned the pylorus slightly above the antrum, a configuration derived from common geometrical representations found in the literature, as referenced in Table 2.12 from Liu.⁴⁵ To further explore the impact of stomach orientation on food emptying dynamics, we have conducted additional simulations with slight adjustments to the model's orientation. These simulations are performed with different directions of gravitational acceleration (g_i), as detailed in Table VI and illustrated in Fig. 14.

The results, shown in Fig. 15(a), indicate that adjusting the orientation from 0° to -60° enhances gastric emptying. This is attributed to the alignment of the stomach outlet more directly with the direction of gravity, facilitating easier emptying of gastric contents. Conversely, changing the orientation from 0° to 60° decreases gastric emptying, as the food settles further from the pylorus and the

**FIG. 15.** (a) The retention rate of the food in the stomach (r_{gr}) and (b) the food on the stomach wall (S_F). The solid line represents the conditions under normal gravity (1G), and the dashed line represents the conditions under zero gravity (0G). The food bolus is initially positioned at location L1.

outlet becomes higher relative to the food, reducing the likelihood of emptying.

Regarding the speed of emptying, our findings reveal that the food empties faster as the orientation changes from 60° to -60° . Compared to the 0G condition and after the initial lag phase, emptying is slower at orientations of 60° , 30° , and 0° , similar to the case at -30° , but faster at -60° . Our numerical results suggest that after the initial lag phase (~ 6 min), food emptying at 0G is faster than at non-0G conditions for most stomach orientations, including the most common orientation.

Furthermore, the variable S_F (the food on the stomach wall) also reflects these dynamics; as the food empties more completely, S_F decreases, as illustrated in Fig. 15(b) after 1200 s. These findings underscore the impact of stomach geometry and orientation on gastric emptying. A wider range of geometrical and positional variations still needs to be studied in future work to ensure the robustness and applicability of our model across different scenarios. In addition, the findings obtained in this study still require further validations with *in vivo* experiments.

REFERENCES

- ¹M. Chen, R. Goyal, M. Majji, and R. E. Skelton, "Design and analysis of a growable artificial gravity space habitat," *Aerosp. Sci. Technol.* **106**, 106147 (2020).
- ²L. Kornilova and I. Kozlovskaya, "Neurosensory mechanisms of space adaptation syndrome," *Hum. Physiol.* **29**, 527 (2003).
- ³H. J. Ortega, D. L. Harm, and M. F. Reschke, *Space and Entry Motion Sickness* (Springer, 2019).
- ⁴M. Shen and W. H. Frishman, "Effects of spaceflight on cardiovascular physiology and health," *Curr. Cardiol. Rev.* **27**, 122 (2019).
- ⁵J.-L. C. Urbain, J. A. Siegel, N. D. Charkes, A. H. Maurer, L. S. Malmud, and R. S. Fisher, "The two-component stomach: Effects of meal particle size on fundal and antral emptying," *Eur. J. Nucl. Med.* **15**, 254 (1989).
- ⁶S. Brandstaeter, S. L. Fuchs, R. C. Aydin, and C. J. Cyron, "Mechanics of the stomach: A review of an emerging field of biomechanics," *GAMM-Mitt.* **42**, e201900001 (2019).
- ⁷G. M. Bornhorst and R. Paul Singh, "Gastric digestion in vivo and in vitro: How the structural aspects of food influence the digestion process," *Annu. Rev. Food Sci. Technol.* **5**, 111 (2014).
- ⁸Y. Li and F. Kong, "Simulating human gastrointestinal motility in dynamic in vitro models," *Compr. Rev. Food Sci. Food Saf.* **21**, 3804 (2022).
- ⁹I. Sensay, "A review on the food digestion in the digestive tract and the used in vitro models," *Curr. Res. Food Sci.* **4**, 308–319 (2021).
- ¹⁰A. Pal, K. Indreshkumar, W. Schwizer, B. Abrahamsson, M. Fried, and J. G. Brasseur, "Gastric flow and mixing studied using computer simulation," *Proc. R. Soc. London, Ser. B* **271**, 2587 (2004).
- ¹¹D. Dufour, F. X. Tanner, K. A. Feigl, and E. J. Windhab, "Investigation of the dispersing characteristics of antral contraction wave flow in a simplified model of the distal stomach," *Phys. Fluids* **33**, 083101 (2021).
- ¹²K. Feigl and F. X. Tanner, "Computational investigation of drop behavior and breakup in peristaltic flow," *Phys. Fluids* **34**(1), 012111 (2022).
- ¹³M. J. Ferrua and R. P. Singh, "Modeling the fluid dynamics in a human stomach to gain insight of food digestion," *J. Food Sci.* **75**, R151 (2010).
- ¹⁴P. Trusov, N. V. Zaitseva, and M. Kamaltdinov, "A multiphase flow in the antroduodenal portion of the gastrointestinal tract: A mathematical model," *Comput. Math. Methods Med.* **2016**, 5164029.
- ¹⁵S. M. Harrison, P. W. Cleary, and M. D. Sinnott, "Investigating mixing and emptying for aqueous liquid content from the stomach using a coupled biomechanical-SPH model," *Food Funct.* **9**, 3202 (2018).
- ¹⁶S. Ishida, T. Miyagawa, G. O'Grady, L. K. Cheng, and Y. Imai, "Quantification of gastric emptying caused by impaired coordination of pyloric closure with antral contraction: A simulation study," *J. R. Soc. Interface* **16**, 20190266 (2019).
- ¹⁷J. H. Seo and R. Mittal, "Computational modeling of drug dissolution in the human stomach," *Front. Physiol.* **12**, 2080 (2022).
- ¹⁸J. H. Lee, S. Kuhar, J.-H. Seo, P. J. Pasricha, and R. Mittal, "Computational modeling of drug dissolution in the human stomach: Effects of posture and gastroparesis on drug bioavailability," *Phys. Fluids* **34**, 081904 (2022).
- ¹⁹S. Kuhar, J. H. Lee, J.-H. Seo, P. J. Pasricha, and R. Mittal, "Effect of stomach motility on food hydrolysis and gastric emptying: Insight from computational models," *Phys. Fluids* **34**, 111909 (2022).
- ²⁰C. Li and Y. Jin, "A CFD model for investigating the dynamics of liquid gastric contents in human-stomach induced by gastric motility," *J. Food Eng.* **296**, 110461 (2021).
- ²¹C. Li, J. Xiao, X. D. Chen, and Y. Jin, "Mixing and emptying of gastric contents in human-stomach: A numerical study," *J. Biomech.* **118**, 110293 (2021).
- ²²C. Li and Y. Jin, "Digestion of meat proteins in a human-stomach: A CFD simulation study," *Innov. Food. Sci. Emerg. Technol.* **83**, 103252 (2023).
- ²³C. Skamniotis, C. H. Edwards, S. Bakalis, G. Frost, and M. Charalambides, "Eulerian-Lagrangian finite element modelling of food flow-fracture in the stomach to engineer digestion," *Innov. Food. Sci. Emerg. Technol.* **66**, 102510 (2020).
- ²⁴G. Tougas, M. Anvari, J. Dent, S. Somers, D. Richards, and G. Stevenson, "Relation of pyloric motility to pyloric opening and closure in healthy subjects," *Gut* **33**, 466 (1992).
- ²⁵C. Skamniotis, M. Elliott, and M. Charalambides, "On modeling the large strain fracture behaviour of soft viscous foods," *Phys. Fluids* **29**, 121610 (2017).
- ²⁶C. Skamniotis and M. Charalambides, "Development of computational design tools for characterising and modelling cutting in ultra soft solids," *Extreme Mech. Lett.* **40**, 100964 (2020).
- ²⁷J. Sicard, P.-S. Mirade, S. Portanguen, S. Clerjon, and A. Kondjoyan, "Simulation of the gastric digestion of proteins of meat bolus using a reaction-diffusion model," *Food Funct.* **9**, 6455 (2018).
- ²⁸K. Schulze, "Imaging and modelling of digestion in the stomach and the duodenum," *Neurogastroenterol. Motil.* **18**, 172 (2006).
- ²⁹M. Einhorn, *Diseases of the Stomach: A Text-Book for Practitioners and Students* (Legare Street Press, 2023).
- ³⁰A. Pal, J. G. Brasseur, and B. Abrahamsson, "A stomach road or "Magenstrasse" for gastric emptying," *J. Biomech.* **40**, 1202 (2007).
- ³¹F. Kong and R. P. Singh, "Disintegration of solid foods in human stomach," *J. Food Sci.* **73**, R67 (2008).
- ³²C. Versantvoort, E. Van de Kamp, and C. Rempelberg, "Development and applicability of an in vitro digestion model in assessing the bioaccessibility of contaminants from food," *Rijksinstituut voor Volksgezondheid en Milieu Report No. 320102002* (2004).
- ³³P. M. Knupp, "Algebraic mesh quality metrics," *SIAM J. Sci. Comput.* **23**, 193 (2001).
- ³⁴J. F. Steffe, *Rheological Methods in Food Process Engineering* (Freeman Press, 1996).
- ³⁵S. K. Singh, *Fluid Flow and Disintegration of Food in Human Stomach* (University of California, Davis, CA, 2007).
- ³⁶M. Holz, S. R. Heil, and A. Sacco, "Temperature-dependent self-diffusion coefficients of water and six selected molecular liquids for calibration in accurate 1H NMR PFG measurements," *Phys. Chem. Chem. Phys.* **2**, 4740 (2000).
- ³⁷E. L. Cussler, *Diffusion: Mass Transfer in Fluid Systems* (Cambridge University Press, 2009).
- ³⁸P. Sheth and J. Tossounian, "The hydrodynamically balanced system (HBS™): A novel drug delivery system for oral use," *Drug Dev. Ind. Pharm.* **10**, 313 (1984).
- ³⁹M. Anvari, M. Horowitz, R. Fraser, A. Maddox, J. Myers, J. Dent, and G. G. Jamieson, "Effects of posture on gastric emptying of nonnutrient liquids and antropyloroduodenal motility," *Am. J. Physiol.: Gastrointest. Liver Physiol.* **268**, G868 (1995).
- ⁴⁰J.-Q. Yang, N. Jiang, Z.-P. Li, S. Guo, Z.-Y. Chen, B.-B. Li, S.-B. Chai, S.-Y. Lu, H.-F. Yan, and P.-M. Sun, "The effects of microgravity on the digestive system and the new insights it brings to the life sciences," *Life Sci. Space Res.* **27**, 74 (2020).
- ⁴¹A. Arzani and S. Shawn C, "Characterizations and correlations of wall shear stress in aneurysmal flow," *J. Biomech. Eng.* **138**, 014503 (2016).
- ⁴²H. Kozu, I. Kobayashi, M. A. Neves, M. Nakajima, K. Uemura, S. Sato, and S. Ichikawa, "PIV and CFD studies on analyzing intragastric flow phenomena

- induced by peristalsis using a human gastric flow simulator," *Food Funct.* **5**, 1839 (2014).
- ⁴³S. Alokaily, K. Feigl, and F. X. Tanner, "Characterization of peristaltic flow during the mixing process in a model human stomach," *Phys. Fluids* **31**, 103105 (2019).
- ⁴⁴Z. Xue, M. J. Ferrua, and P. Singh, "Computational fluid dynamics modeling of granular flow in human stomach," *Aliment. Hoy* **21**, 3 (2012).
- ⁴⁵X. Liu, "Verification and validation of numerical modelling approaches pertinent to stomach modelling," Ph.D. dissertation (The University of Sydney, 2023).